



Original Research

A gap-filling, regenerative implant for open-wedge osteotomy

Margot Rikkers^{a,*}, H. Chien Nguyen^{a,b,#}, Nasim Golafshan^{a,#}, Mylène de Ruijter^a,
Riccardo Levato^{a,c}, Lucienne A. Vonk^{a,d}, Nienke van Egmond^a, Miguel Castilho^{a,e},
Roel J.H. Custers^a, and Jos Malda^{a,c,*}

^a Department of Orthopaedics, University Medical Center Utrecht, Utrecht, The Netherlands

^b 3D Lab, University Medical Centre Utrecht, Utrecht, the Netherlands

^c Department of Clinical Sciences, Faculty of Veterinary Medicine, Utrecht University, Utrecht, The Netherlands

^d Xintela AB, Lund, Sweden

^e Orthopaedic Biomechanics, Department of Biomedical Engineering, Eindhoven University of Technology, Eindhoven, The Netherlands



ARTICLE INFO

Keywords:

Implant

Magnesium phosphate

Open wedge

Osteotomy

Osteoinductive

3D printing

ABSTRACT

Introduction: In patients suffering from unilateral osteoarthritis in the knee, an osteotomy can provide symptomatic relief and postpone the need for replacement of the joint. Nevertheless, open-wedge osteotomies (OWOs) around the knee joint face several challenges like postoperative pain and bone nonunion.

Objectives: In this study, the aim was to design, fabricate, and evaluate a gap-filling implant for OWO using an osteoinductive and degradable biomaterial.

Methods: Design of porous wedge-shaped implants was based on computed tomography scans of cadaveric legs. Implants were 3-dimensionally printed using a magnesium strontium phosphate-polycaprolactone (MgPSr-PCL) biomaterial ink. Standardized scaffolds with different inter-fiber spacing (IFS) were mechanically characterized and osteoinductive properties of the biomaterial were assessed in vitro. Finally, human-sized implants with different heights (5 mm, 10 mm, 15 mm) were designed and fabricated for ex vivo implantation during 3 OWO procedures in human cadaveric legs.

Results: Implants printed with an interior of IFS-1.0 resulted in scaffolds that maintained top and bottom porosity, while the interior of the implant exhibited significant mechanical stability. Bone marrow concentrate and culture expanded mesenchymal stromal cells attached to the MgPSr-PCL material and proliferated over 21 days in culture. The production of osteogenic markers alkaline phosphatase activity, calcium, and osteocalcin was promoted in all culture conditions, independent of osteogenic induction medium. Finally, 3 OWO procedures were planned and fabricated wedges were implanted ex vivo during the procedures. A small fraction of one side of the wedges was resected to assure fit into the proximal biplanar osteotomy gap. Preplanned wedge heights were maintained after implantation as measured by micro-computed tomography.

Conclusion: To conclude, personalized implants for implantation in OWOs were successfully designed and manufactured. The implant material supported osteogenesis of mesenchymal stromal cells and bone marrow concentrate in vitro and full-size implants were successfully implemented into the surgical procedure without compromising preplanned wedge height.

* Department of Orthopaedics, University Medical Center Utrecht, Heidelberglaan 100, Utrecht, 3584 CX, the Netherlands.

Email addresses: margotrikkers@gmail.com (M. Rikkers), j.malda@umcutrecht.nl (J. Malda).

These authors contributed equally.

Introduction

Unicompartmental knee osteoarthritis is often associated with lower limb malalignment. Especially for younger patients (age <65 years) with unicompartmental osteoarthritis and a malalignment, a correctional osteotomy can be a surgical solution, aiming to unload the affected compartment.¹⁻³

While open-wedge osteotomies (OWOs) and closing-wedge osteotomies (CWOs) have shown comparable clinical outcome,^{4,5} OWOs have gained popularity over CWOs in the tibia, mainly due to practical considerations. When performing a CWO in the tibia, an osteotomy of the fibula is necessary and future conversion to a partial or total knee arthroplasty is complicated.⁶ But not without importance, medial high tibial OWO remains associated with pain in the early postoperative stage and has a higher risk for delayed or non-union.^{7,8} Postoperative pain is believed to be (at least in part) caused by bone marrow leakage from the osteotomy site, causing swelling, resulting in impaired early weight-bearing, ambulation, and rehabilitation.⁹

In some cases, the opened osteotomy wedge is filled with an autologous bone graft from the iliac crest.¹⁰ However, this procedure is aimed at accelerating union rather than closing the gap and it is associated with donor site morbidity.¹¹ Filling the osteotomy gap with an allogeneic bone graft could be a viable solution as gap filler and has demonstrated improved pain levels after the procedure compared to baseline in a case series of 103 patients.⁸ Almost all of the patients (99%) were able to walk >500 meters without any support 3 months after surgery. However, the use of allogeneic bone grafts is hampered by the limited availability of the grafts. Moreover, frozen allografts were shown to have a higher failure rate (defined as construct failure or non-union) compared to living autologous grafts.¹² Alternatively, synthetic bone substitutes made of hydroxyapatite or beta-tricalcium phosphate^{7,13-15} aid in bone union without donor site morbidity. Nevertheless, most bone substitute wedges are not designed to imitate the structure of trabecular bone with a dense cortical border. To improve bone union, postoperative pain, and eliminate the need for an allograft or autograft in OWO procedures, a firm, gap-filling 3-dimensional (3D)-printed scaffold with osteoconductive properties and mechanical stability provides a solution.

Among the bioactive ceramic materials that have been used for bone tissue engineering, magnesium strontium phosphate (MgPSr) has gained particular interest due to the good solubility of magnesium phosphate phases under physiological conditions, and the presence of Sr^{2+} ions have been demonstrated to promote osteogenic differentiation of mesenchymal stromal cells (MSCs).¹⁶⁻²¹ However, pure ceramic scaffolds are usually brittle and prone to fracture which hampers their application in large, load-bearing defects.²² A previous study has investigated a ceramic-polymer composite of MgPSr and polycaprolactone (PCL), which is a versatile biomaterial ink that can be processed through extrusion-based 3D printing at room temperature. The biomaterial can be manufactured into different complex geometries to improve bone filling of a defect without compromising mechanical stability.²³ The porous nature of a printed osteotomy wedge scaffold allows bone marrow to populate the wedge upon implantation. Alternatively, presurgical seeding of the implant with a bioactive product accelerating osteogenesis, such as bone marrow concentrate (BMC), could further accelerate bone union.

This study aimed to design and manufacture a scaffold as gap filler in OWO around the knee joint. The mechanical stability of the wedge scaffold, as well as the in vitro osteoinductive properties of the material on MSCs and BMC were investigated. Additionally, preservation of the predesigned implant structure and height were assessed upon implantation into human cadaveric legs.

Materials and methods

Study outline

To completely fill the opening wedge gap after an OWO, 3D printed scaffolds were manufactured using patient computed tomography (CT) data and computer-aided design (CAD). The printed scaffold structures were mechanically characterized and in vitro potency of the MgPSr-PCL material was evaluated to induce osteogenesis when seeded with bone marrow-derived MSCs, as well as BMC. Finally, a proof-of-concept surgical implantation in a cadaver model was performed for implementation of the implants into the current osteotomy procedure.

CAD of osteotomy wedge

For initial design of a wedge scaffold for mechanical characterization and in vitro experiments, an anonymized CT scan and surgical planning for an 8 mm medial opening-wedge distal femur osteotomy was acquired from a clinical case (University Medical Center Utrecht) (Fig. 1Ai). The CAD of the wedge scaffold was developed in SolidWorks software (Dassault Systèmes), using the CT scan images. After assessment of the wedge scaffold, BioCAM software was used to define the wedge scaffold internal architecture and subsequently translate the design into a G-Code. The external wall of the osteotomy scaffold was kept closed with 2 outer layers, while for the internal region of the osteotomy scaffolds, 3 different inter-fiber spacings (IFSs), 1.3 mm, 1.0 mm, and 0.7 mm (IFS-1.3, IFS-1.0, and IFS-0.7, respectively) were considered.

Material preparation and extrusion-based 3D-bioprinting

The biomaterial ink was prepared by combining in-house synthesized $\text{Mg}_{2.33}\text{Sr}_{0.67}(\text{PO}_4)_2$ powder and commercial medical grade poly(ϵ -caprolactone) (mPCL, Purasorb PC 12, Purac Biomaterials) in a weight ratio of 70:30 wt.% of MgPSr to PCL, according to a procedure previously described.²³ Designed scaffolds were fabricated by an extrusion-based 3D-printing system (3D Discovery,

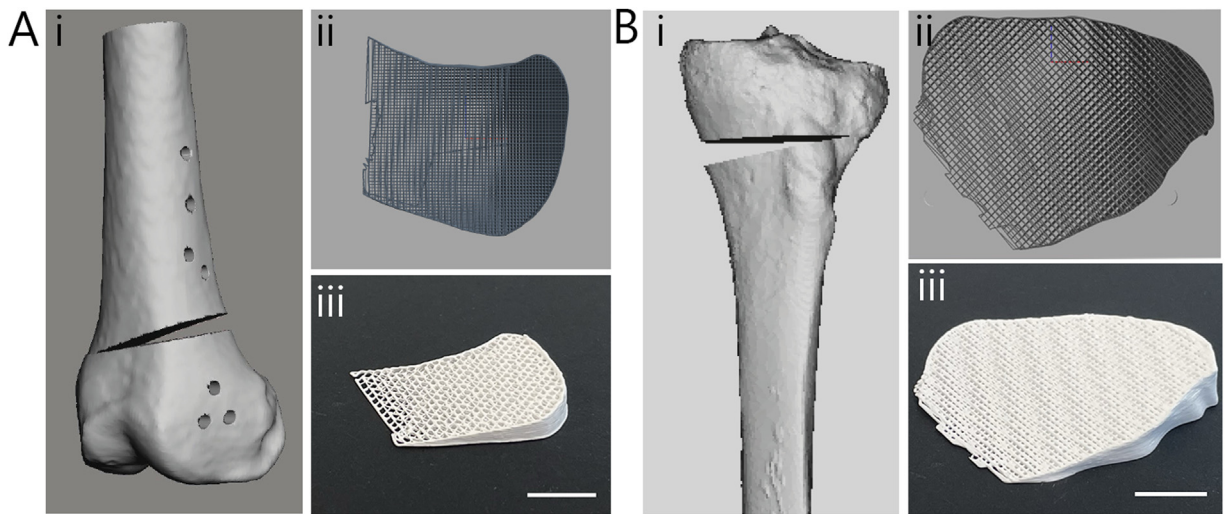


Fig. 1. Surgical planning and extrusion-based printing. Wedge design for open-wedge osteotomies in distal femur (A) and proximal tibia (B). **Panels i**, Surgical planning of open-wedge osteotomies derived from computed tomography scans. **Panels ii**, Top views of printing paths of computer-aided designs of personalized wedge implants. **Panels iii**, The finalized personalized wedges in magnesium strontium phosphate-polycaprolactone biomaterial. Scale bar = 10 mm.

regenHU) using the MgPSr-PCL biomaterial ink. The ink was transferred to a 10 mL syringe (Nordson EFD) and extruded through a 22G conical nozzle (inner diameter = 0.41 mm; Nordson EFD) at a pressure of 0.9 bar and collected at collector speed of 6 mm/s.

Mechanical characterization of printed wedge scaffolds

Uniaxial compression tests were performed using a universal testing machine (Zwick Z010) equipped with a 1 kN load cell. Tests were performed on cylindrical samples ($d = 6$ mm, $h = 12$ mm, $n = 5$) for all 3 groups (IFS-1.3, IFS-1.0 and IFS-0.7, without closed outer edges), at a rate of 1 mm/min (at room temperature). From the engineered stress-strain curves, the elastic modulus (defined as the slope of the linear region at the interval 0.02–0.05 mm/mm strain), the yield stress (defined as the point where nonlinear deformation begins), and toughness (defined as the absorbed energy by the scaffolds up to yield stress) were determined.

In vitro accelerated degradation of printed wedge scaffolds

The degradation of the materials was studied under controlled conditions which accelerated biomaterial degradation in vitro.²² Wedge scaffolds were incubated in a 0.4 mg/ml lipase solution (from *Pseudomonas cepacia*, Sigma-Aldrich) and 1 mg/ml sodium azide (Sigma-Aldrich) at 37°C for 15 days. At each time point (1, 5, 10, and 15 days), the enzymatic solution was refreshed, and samples were monitored for weight loss, quantified as per Eq. (1):

$$\text{Weight loss} = \frac{W_{D15} - D_0}{D_0} \quad (1)$$

In vitro osteogenesis of scaffolds

Donors and cell isolation

Human bone marrow-derived mesenchymal stromal cells were derived from healthy donor bone marrow aspirates ($n = 3$, age range 2–12) as approved by the Dutch Central Committee on Research Involving Human Subjects (CCMO, Bio-banking bone marrow for MSC expansion, NL41015.041.12). The parent or legal guardian of the donor signed the informed consent approved by the CCMO. In brief, the mononuclear fraction was separated using a density gradient (Lymphoprep, Axis Shield). MSCs were isolated by plastic adherence and expanded for 3 passages in Minimum Essential Media (α MEM, Macopharma) with 5% platelet lysate and 3.3 IU/mL heparin and cryopreserved. Subsequently, MSCs were expanded for 2 additional passages in MSC expansion medium (α MEM [Gibco], 10% (v/v) fetal bovine serum [FBS; Biowest], 1% penicillin/streptomycin [pen/strep; 100 U/mL, 100 μ g/mL], 200 μ M l-ascorbic acid 2-phosphate [ASAP; Sigma-Aldrich], and 1 ng/mL basic fibroblast growth factor [bFGF; PeproTech]). BMC was obtained from donors undergoing an OWO or total knee arthroplasty surgery ($n = 2$, age range 39–49 years) after their signed informed consent was received (protocol approved by the local medical ethical committee). Bone marrow was concentrated to one tenth of its original volume using Ficoll paque (GE Healthcare) density separation.

In vitro culture of scaffolds

Standardized 5 mm diameter cylindrical scaffolds (ISF-1.0) were printed as described before²³ and sterilized by washing in 70% ethanol and Milli-Q, followed by exposure to ultraviolet light for 1 hour. Scaffolds were cut in half with a sterile scalpel and seeded with either 15,000 MSCs/scaffold in fibrin gel (25 μ L fibrinogen [1:15 in phosphate-buffered saline {PBS}] crosslinked with 25 μ L thrombin (1:50 in PBS); Tisseel, Baxter) or 25 μ L BMC (crosslinked with 16.6 μ L thrombin and 16.6 μ L CaCl₂ [500 mM in 0.9% NaCl]). Cell-seeded scaffolds were precultured in MSC expansion medium for 2 days, followed by 21 days of osteogenic induction with osteogenic differentiation medium (α MEM supplemented with 10% FBS, 1% pen/strep, 200 μ M ASAP, 10 mM β -glycerophosphate [Sigma-Aldrich], and 10 nM dexamethasone [Sigma-Aldrich]). Control cell-seeded scaffolds were treated with MSC expansion medium without bFGF.

Alkaline phosphatase, calcium, and DNA quantification

Osteogenic differentiation of the cells was measured by the activity of the early osteogenic marker alkaline phosphatase (ALP) after 5, 7, and 11 days and by quantification of calcium produced after 21 days. To determine activity of ALP, cells were lysed in Tris-EDTA buffer (10 mM Tris-HCl, 1 mM EDTA, pH 8) by 3 freeze-thaw cycles. ALP activity was measured using the conversion of p-nitrophenyl phosphate liquid substrate (pNPP, Sigma-Aldrich). Absorbance was measured every minute for 30 minutes at 405 nm and corrected for absorbance at 655 nm. Calf intestinal ALP (Sigma-Aldrich) was used as a standard. Calcium concentration in the samples was quantified after 21 days using a colorimetric calcium assay kit (Abcam) according to the manufacturer's instructions. ALP activity and calcium levels were corrected for DNA. DNA content was determined using the Quant-iT PicoGreen dsDNA assay (Invitrogen) according to the manufacturer's instructions.

Osteocalcin immunocytochemistry

To visualize the osteogenic marker osteocalcin, scaffolds were fixed in formalin for 30 minutes for the osteocalcin immunocytochemistry after 21 days of differentiation. Samples were permeabilized with 0.2% (v/v) Triton X-100 in PBS, followed by blocking with 5% (v/v) bovine serum albumin in PBS. Next, samples were incubated overnight at 4°C with 10 μ g/mL mouse-anti-human primary antibody against osteocalcin (clone OCG4; Enzo Life Sciences). Samples were then incubated with 10 μ g/mL goat-anti-mouse antibody conjugated to Alex Fluor 488 (Invitrogen) for 1 hour at room temperature. All samples were also stained for F-actin (1:200; phalloidin-TRITC; Sigma-Aldrich) and 4',6-diamidino-2-phenylindole (100 ng/mL; DAPI; Sigma-Aldrich). Images were acquired with a Leica SP8X Laser Scanning Confocal Microscope and Leica LASX acquisition software.

Ex vivo surgical implantation of the printed wedges

Three fresh-frozen human cadaveric legs were obtained (all left legs, one male and 2 female) in accordance with the guidelines of the local medical ethical committee. CT scans were obtained of the 3 included legs (Philips Healthcare; 100 kV and 130 mAs), with 0.8 mm slice thickness. Single plane OWOs were preoperatively planned in 3-Matic (Materialise), with a specific wedge height for each leg (5, 10, and 15 mm). This resulted in postsurgical 3D-models of the cadavers with left open osteotomy gaps, which functioned as surrogate for the 3D printing of the wedges. A proximal biplanar medial high tibial OWO was performed following a standard surgery protocol. During this procedure, the osteotomy gap was kept open using a lamina spreader and the 3D-printed scaffold wedge was inserted into the gap. The tips of the wedge scaffolds were resected to fit the biplanar osteotomy gap, without altering the outside rim of the wedge. The osteotomies were then fixated with angular stable plates (Activmotion, Newclip Technics). The same plates are used for patients in the clinic and have a smaller footprint compared to other commercially used plates. Following implantation of the scaffold wedges, additional CT scans were obtained of the operated cadaver legs; subsequently the wedges were explanted for further analysis.

Micro-CT

The pre- and postsurgical wedge scaffolds underwent micro-CT (Quantum FX-Perkin Elmer) for height analyses. Scan parameters were 90 kV tube voltage, 180 μ A tube current, 60 or 73 mm resolution, and 2 minute scan time. Scaffold heights pre- and postimplantation were quantified using computer vision software Fiji (software version 2.1.0/1.53c, National Institutes of Health). Scaffold height was measured at the highest point. The micro-CT images of a single scaffold pre- and postimplantation were superimposed to ensure the scaffolds were measured at the same location at both timepoints.

Statistical analysis

Statistical analyses were performed using GraphPad Prism 8.3 (GraphPad Software, Inc.). All data were presented as mean \pm SD. To test for differences in mechanical evaluations and calcium content, a one-way analysis of variance (ANOVA) with Tukey's post hoc test was used. To test for differences in DNA and ALP quantifications, a two-way ANOVA with Tukey's post hoc was used. For scaffold wedge height, a two-tailed *t* test was used. Normality was confirmed with a Shapiro-Wilk test (*P* > .05). *P* values below .05 were considered significant.

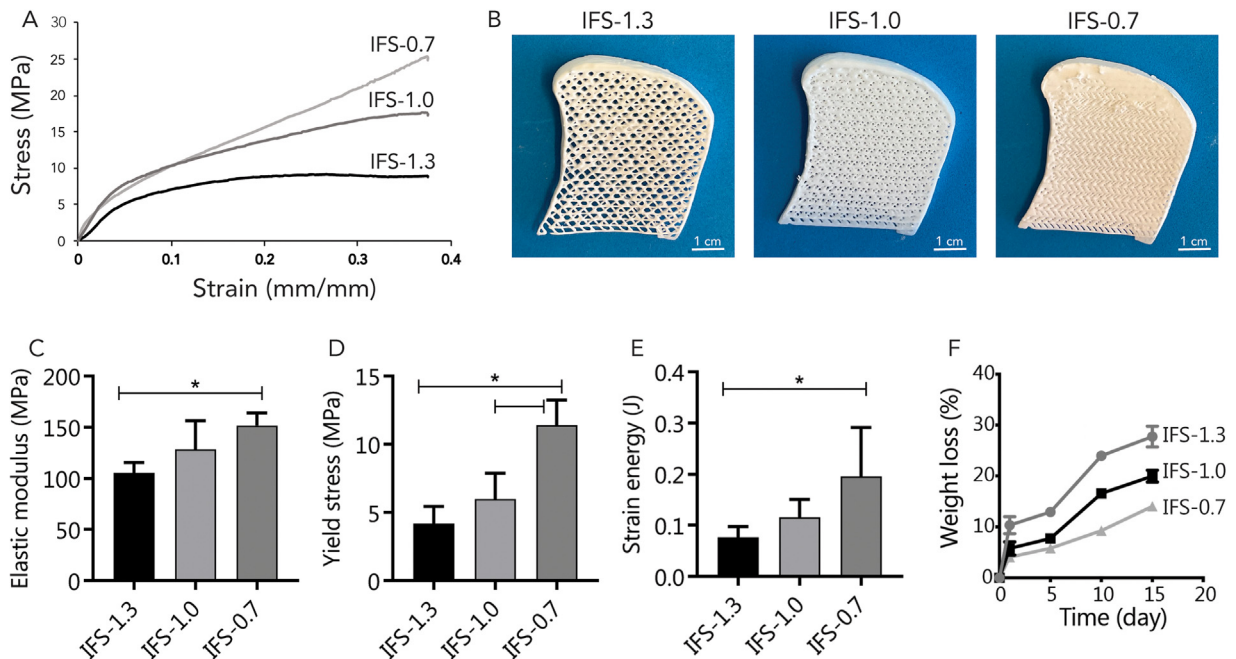


Fig. 2. Evaluation of mechanical properties of the printed magnesium strontium phosphate-polycaprolactone (MgPSr-PCL) wedges. **A**, Longitudinal compression profile of 3D printed MgPSr-PCL wedge scaffolds for inter-fiber spacing (IFS)-1.3, IFS-1.0, and IFS-0.7. **B**, Corresponding photographs showed the different scaffolds after the printing. Open pores in wedges IFS-1.3 and IFS-1.0 can be appreciated, while IFS-0.7 wedges were not porous. Elastic modulus **C**, yield stress **D**, and strain energy **E**, from compressive loading profile for IFS-1.3, IFS-1.0, and IFS-0.7. **F**, Weight loss of wedge scaffolds during accelerated in vitro degradation in enzymatic solution over 15 days. * $P < .05$.

Results

Personalized implant design and fabrication

Wedge implants were designed for both open-wedge lateral distal femur (for in vitro analyses; Fig. 1A) and medial tibial osteotomies (for implantation in cadavers; Fig. 1B) from CT scan 3D reconstructions (Fig. 1 Panels i). Wedges had closed outer edges, aimed at limiting leakage from the osteotomy site into the soft tissues surrounding the bone, while the interior was porous (Fig. 1 Panels ii and iii).

Mechanical profile of printed porous material

Incorporation of the thermoplastic PCL into the ceramic MgPSr phase improved handling of the implants, overcoming downsides of brittle ceramic materials.²² The stress-strain curves of the standardized printed discs with different IFS showed comparable profiles (Fig. 2A). The decrease in IFS resulted in an increase in mechanical stability, elastic modulus increased significantly from 105.3 ± 10.26 MPa (IFS-1.3) to 151.5 ± 12.61 MPa (IFS-0.7) (Fig. 2C). Yield stress, defined as the point of maximum elastic deformation, increased from 4.2 ± 1.27 MPa (IFS-1.3) to 6.0 ± 1.90 MPa and 11.4 ± 1.86 MPa for IFS-1.0 and IFS-0.7, respectively (Fig. 2D). In line, strain energy increased from 0.077 ± 0.0208 J for IFS-1.3 to 0.196 ± 0.0957 J for IFS-0.7 (Fig. 2E). Although a disc with an IFS of 0.7 mm presented the highest elastic modulus, printing of a complete wedge scaffold with this IFS resulted in a construct that was not completely porous from top to bottom, which is essential to flow of bone marrow through the scaffold in vivo (Fig. 2B). Scaffolds with a planned IFS of 1.0 mm resulted in completely porous wedges and only a slight difference in elastic modulus and strain energy compared to scaffolds with a planned IFS of 0.7 mm, which did not reach statistical significance. While the degradation rate of IFS-1.3 samples (as evaluated under accelerated degradation conditions) was 30% faster compared to IFS-1.0 samples (Fig. 2F), the combination of tested characteristics led to the selection of IFS-1.0 for further analyses as the best compromise between open porosity, mechanical stability, and degradation properties.

In vitro osteogenic properties of the scaffold material

Human bone marrow-derived mesenchymal stromal cells embedded in fibrin (MSC-fibrin) were seeded in the biomaterial scaffolds to evaluate osteogenic potential. Additionally, to simulate the in vivo situation, a second group of scaffolds was seeded with BMC. The culture-expanded human MSCs attached to the MgPSr-PCL material and proliferated over time. Cells in BMC also proliferated on the

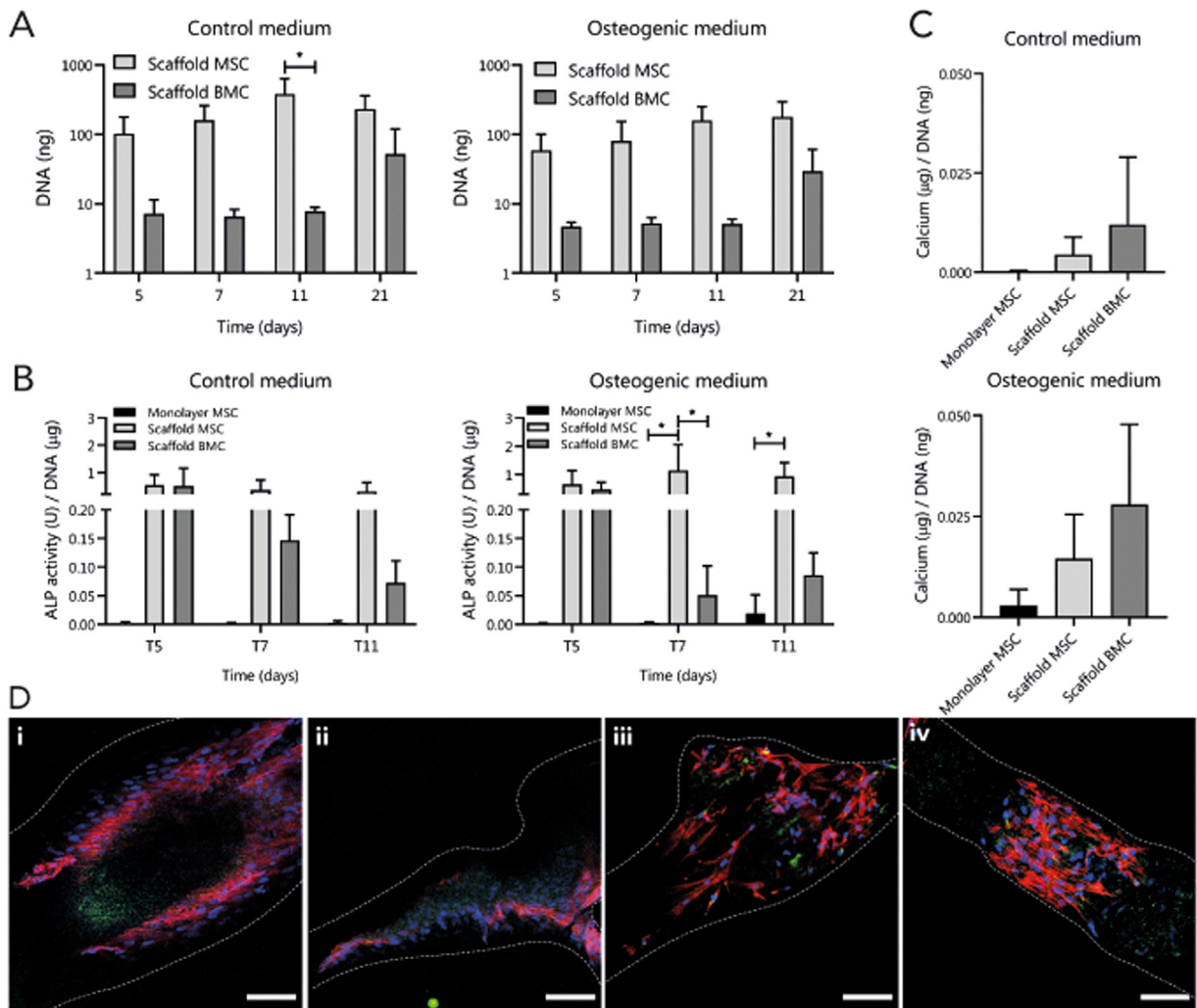


Fig. 3. In vitro osteogenic performance of the magnesium strontium phosphate-polycaprolactone (MgPSr-PCL) biomaterial. **A**, Quantification of DNA in the MgPSr-PCL scaffolds at 5, 7, 11, and 21 days in culture with control (left panel) and osteogenic medium (right panel). **B**, Early osteogenic marker alkaline phosphatase (ALP) activity relative to the amount of DNA at 5, 7, and 11 days. **C**, Calcium content of the cultured constructs at day 21 in control medium (top panel) and osteogenic medium (bottom panel). **D**, Immunocytochemical osteocalcin staining on 21-day cultured standardized cylindrical MgPSr-PCL scaffolds (ISF-1.0) using: culture expanded mesenchymal stromal cells (MSC) in control medium (i), MSC in osteogenic medium (ii), bone marrow concentrate (BMC) in control medium (iii), and BMC in osteogenic medium (iv). Nuclei are shown in blue (DAPI), osteocalcin expression in green, and F-actin in red. Dashed lines indicate the location of three-dimensional scaffold material. Scale bar = 100 µm. * $P < .05$.

scaffolds (Fig. 4A and Fig. S1). Activity of the early osteogenic marker ALP was similar in MSC-fibrin and BMC groups when scaffolds were cultured in control medium, yet were increased in MSC-fibrin when cultured in osteogenic medium (Fig. 4B). BMC performed similar to MSC-fibrin in terms of calcium production at 21 days of culture (Fig. 4C). Of note, both experimental groups had a higher ALP activity and increased calcium production compared to MSCs that were cultured in monolayers, indicating osteoconductive effects of the scaffold material and 3D environment. Production of osteocalcin, an exclusive marker for osteoblasts, was observed in cultures under all conditions irrespective of culture medium used (Fig. 3D).

Ex vivo surgical implantation

Three fresh-frozen human cadaveric legs underwent CT scanning in order to plan 3 OWOs with different heights: 5, 10, and 15 mm (Fig. 4A-C). 3D models of the tibias were used to plan single plane osteotomy gap (Fig. 4 Panels i) and design the wedge scaffolds (Fig. 4 Panels ii). Wedges were implanted during a standard proximal biplanar OWO procedure and fixated with an angular stable plate (Fig. 4 Panels iii). Postsurgical X rays (Fig. 4 Panels iv) and CT scans (Fig. 4 Panels v) illustrate the scaffold positioning and fit. Micro-CT analyses of the wedges pre- and postimplantation indicated good analogy of the scaffolds (Fig. 5A, preoperative in red,

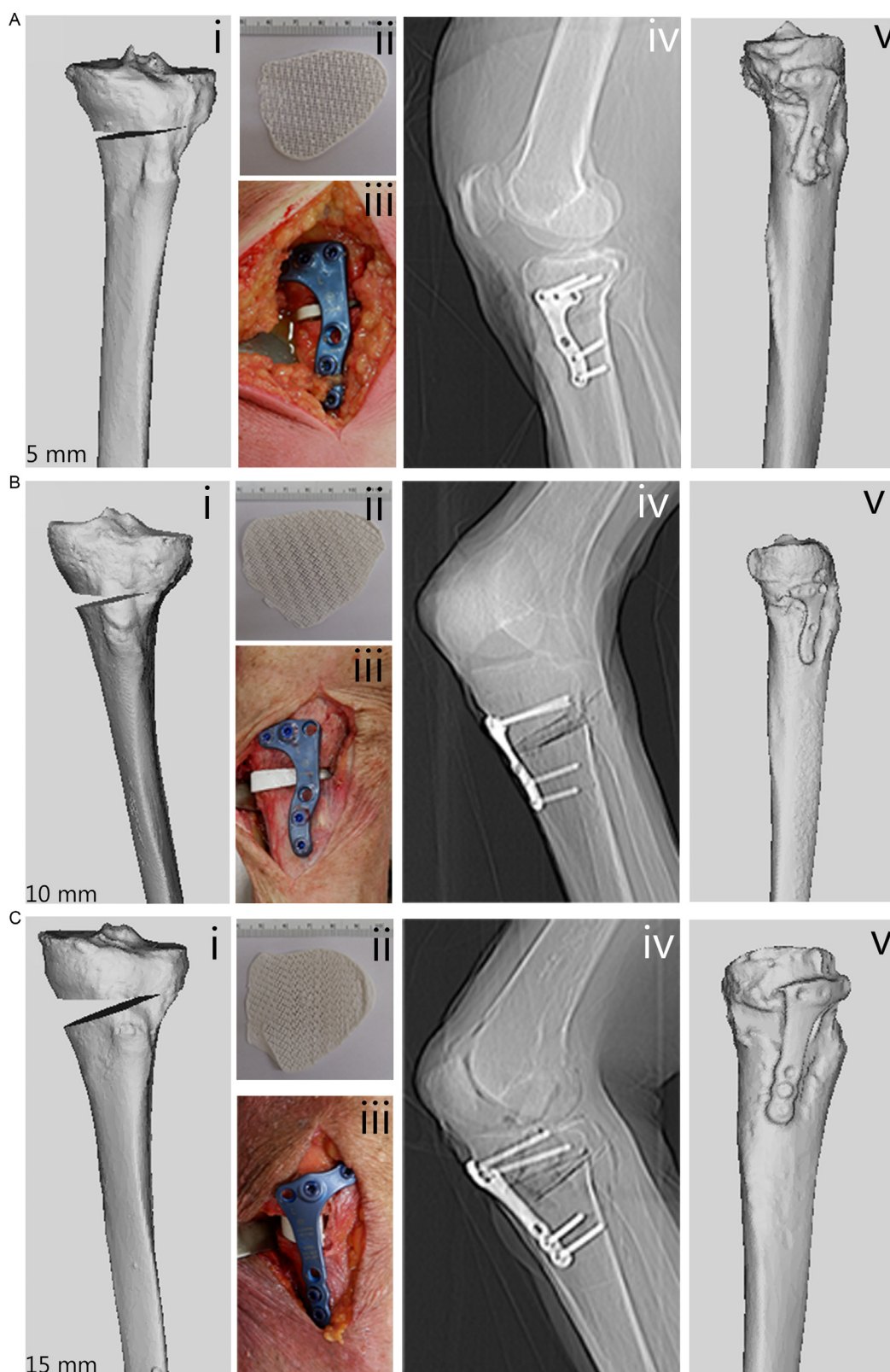


Fig. 4. Surgical implantation of personalized scaffold wedges. Planned osteotomy heights of 5 mm **A**, 10 mm **B**, and 15 mm **C** from computed tomography (CT) scans of human cadaveric legs **Panels i**. **Panels ii**, Three-dimensional (3D) printed wedge scaffolds in magnesium strontium phosphate-polycaprolactone. **Panels iii**, Scaffolds implanted in the cadaveric legs. **Panels iv**, X-ray of the legs after implantation. **Panels v**, 3D reconstruction from CT scans after implantation of the wedge scaffolds.

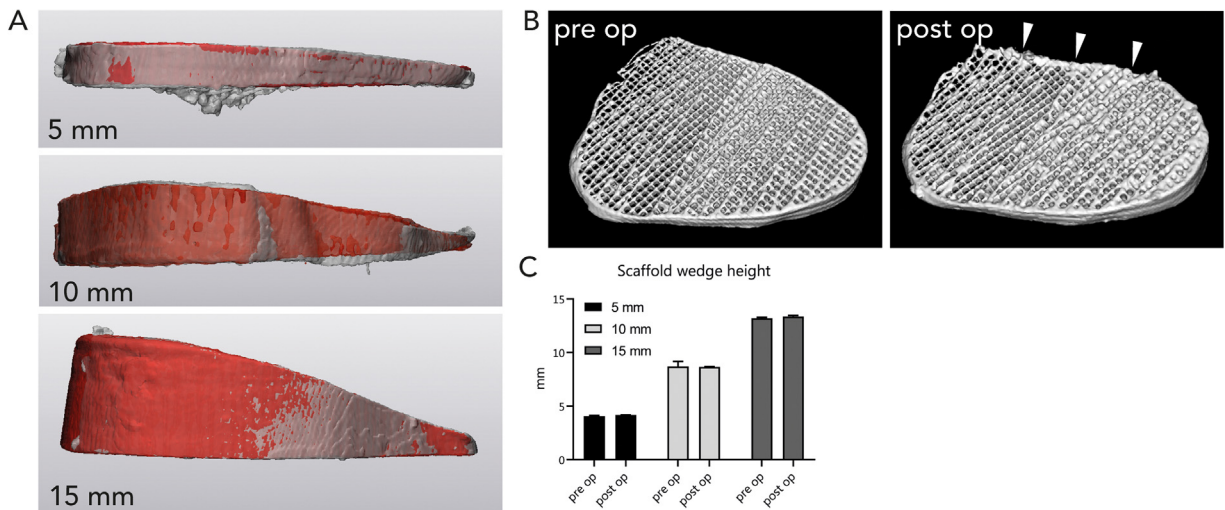


Fig. 5. Micro-computed tomography (CT) analysis of printed wedge scaffolds. **A**, Three-dimensional reconstructions of the wedges from micro-CT images of the printed wedges pre- and postimplantation. Preimplanted scaffolds are in red; postimplanted scaffolds are in gray. **B**, Micro-CT reconstruction of the 5 mm wedge. Note the small portion that was adjusted during the procedure (indicated by the white arrow heads). **C**, Quantification of scaffold wedge height before and after implantation into the cadaveric legs revealed no loss of scaffold height. Post op, postoperative; pre op, preoperative.

postoperative in gray). Due to the biplanar approach of the osteotomy procedure,²⁴ the scaffolds were adjusted at one side using an automatic saw, not altering the rest of the scaffold shape and outer rim (Fig. 5B, arrows indicating trimmed edge). Quantification of wedge heights from micro-CT images revealed that the wedge heights were not affected by the applied surgical procedure, during which they bear loading for a brief moment when the laminar spreader is removed to allow sufficient space for the plate to be fixated (Fig. 5C).

Discussion

This study demonstrated a proof of concept to manufacture implants for bone gap filling in femoral or tibial OWOs, by 3D printing a biodegradable and osteoinductive scaffold material. The printed material promoted osteogenesis of MSCs and BMC in vitro and scaffolds were implanted ex vivo without compromising preoperatively planned wedge height. The aim was to design implants that fitted the planned osteotomy gap and height, fabricate these, and evaluate their implementation in the established surgical procedure.

Postsurgical pain poses a challenge in OWO care. One of the hypotheses for the cause of pain is bleeding from the osteotomy site. It has been shown that fitting an allogeneic graft, which closes the gap completely, enables early postoperative weight-bearing and improved clinical outcomes after 3 months.⁸ A variety of scaffold materials and growth factors is being investigated to accelerate osteogenesis in OWO. Most studies investigating a scaffold material make use of wedges composed of hydroxyapatite or beta-tricalcium phosphate,^{7,14,25} whereas some focus on injection of biologics, like platelet-rich plasma and MSCs,²⁶ or use a single growth factor, like bone morphogenetic protein 6.²⁷

Although a great deal of effort is put into accelerating bone healing, the current study investigates a combined approach of osteoinduction and filling of the osteotomy gap. The presented methods offer the possibility of personalizing an osteoinductive wedge implant and incorporating this into the existing 3D workflow. Yet, the manufactured implants were designed to match opening-wedge height and the anatomy of the bone. Adjustment of the scaffold edge enabled proper fit into the osteotomy plane, while still filling the gap. Precisely sealing the whole gap was proven to be challenging in the current setup. The approach used in the current study led to a relatively symmetrical wedge, as opposed to a trapezoid-shaped wedge. To move towards clinical implementation and complete sealing of an osteotomy gap, a more precise, biplanar surgical planning should be performed. Most likely, this would also require using 3D printed patient-specific instruments (PSI), with preoperatively determined saw cuts resulting in a predefined gap morphology, for which a fitting implant subsequently can be fabricated. In some cases of malalignment correction, PSI are preferred by orthopedic surgeons, in the form of saw and drill guides preoperatively. Further research can offer the possibility of adding a personalized wedge implant into this workflow. With predetermined bone cuts and gap morphology, our wedge scaffold can be 3D printed preoperatively to fit. However, this initial study focused primarily on the feasibility of implanting a 3D printed MgPSr-PCL wedge scaffold without compromising the preoperatively planned wedge height.

Since most of the load on the osteotomy gap is absorbed by the angular stable plate and screws, the implant should remain stable during the brief period before the plate is fixed on the bone. The elastic modulus of the implants demonstrated similarities to human trabecular bone.²⁸ Scaffolds with a planned fiber spacing of 1.0 mm maintained open pores, through which bone marrow would be allowed to flow and osteogenesis might be accelerated. Although implant height was maintained postimplantation in the cadaveric

legs, future in vivo and clinical studies are necessary to confirm maintenance of preplanned wedge height during a longer period of implantation, as well as speed of bone union.

The full-size implants degraded over time in an accelerated in vitro setup using an enzymatic solution. Prior research in an equine model has shown that degradation of the MgPSr-PCL (pore size 1.0 mm) in the enzymatic solution for 10 days corresponded to degradation over 6 months during in vivo implantation.²³ Increasing IFS accelerated degradation by 30% in mass loss, indicating that in vivo mass loss might also be accelerated. However, the exact degradation and speed of bone formation of the osteotomy-specific MgPSr-PCL implants in this specific anatomical location should be evaluated in a large animal model.

The printed MgPSr-PCL material facilitated osteogenesis in vitro, confirming previous findings.²³ For large defects, preseeding of the scaffold with a regenerative compound, like MSCs, might be beneficial to accelerate bone healing. Here, seeding of the material with both culture-expanded MSCs and BMC resulted in production of osteoblast-specific markers, indicating that infiltrated bone marrow in the scaffold material after implantation may be sufficient by itself to stimulate osteogenesis. This is most likely induced by its growth factor-rich nature and the presence of progenitor cells.²⁹ While fabrication of personalized 3D implants from patient imaging data was demonstrated before for orthopedic applications,^{30,31} this study is the first to our knowledge to report on a personalized biodegradable implant for OWO.

The current study was mainly limited by the imbalance between preoperative osteotomy planning (single plane) and the intra-operative surgical biplanar osteotomy, leading to a slight mismatch between gap and fabricated implant. By implementing 3D printed PSI in the workflow, an optimal fit of the designed implant can be achieved. Because the purpose of this study was to design and manufacture a gap-filling wedge implant in an osteoinductive material and to evaluate this in an ex vivo model, achieving a perfect fit was beyond the scope of this investigation.

Conclusions

To conclude, a gap-filling implant for OWOs was designed and manufactured. This implant was 3D manufactured in an osteoinductive and biodegradable material that supported cell attachment, growth, and production of early and late osteogenic markers in vitro. Finally, an ex vivo proof-of-concept of the surgical procedure was successfully performed, implementing the designed wedge scaffolds into the standard osteotomy procedure, while maintaining implant integrity and preplanned wedge height.

Funding

This research is supported by the partners of Regenerative Medicine Crossing Borders, financed by the Dutch Ministry of Economic Affairs by means of the public-private partnership allowance made available by the Top Sector Life Sciences & Health to stimulate public-private partnership, and ReumaNederland (LLP-12, LLP22, and 19-1-207 MINIJoint). J.M. and M.C. acknowledge financial support from the Gravitation Program “Materials Driven Regeneration,” funded by the Netherlands Organization for Scientific Research (024.003.013). M.C. also acknowledges funding from Reprint project (OCENW.XS5.161) by Netherlands Organization Scientific Research.

Ethics approval

This research did not include any human subjects and therefore no written consent was necessary to be obtained. The parent or legal guardian of the donor signed the informed consent approved by the CCMO.

Authorship contributions

L.A.V., N.vE., R.J.H.C., and J.M. conceived the study. All authors were involved in design of the study. M.R., N.G., and M.dR. carried out the laboratory experiments. N.G. and M.C. prepared the biomaterial ink. M.R., H.C.N., N.vE., and R.J.H.C. were involved in the cadaver study. M.R., H.C.N., and N.G. drafted the article. All authors revised the article critically and have given final approval of the version to be published.

Declaration of competing interest

The authors declare that they have no competing interests. L.A.V. is currently employed by Xintela AB.

Acknowledgments

The authors thank Arno Mooring (iMoveMedical, Nieuwegein, The Netherlands) for providing surgical tools and the 3D Lab of the University Medical Center for their assistance in planning of the osteotomies. The authors also thank Nils van Veen for assisting with the CT scans and Marco Rondhuis for his kind assistance at the Anatomy Department. The authors also thank Dr. Elke Vorndran and Prof. Uwe Gbureck from the Department for Functional Materials in Medicine and Dentistry, University of Würzburg, for kindly synthesizing and providing the ceramic biomaterial used in this work.

Supplementary materials

Supplementary material associated with this article can be found, in the online version, at doi:[10.1016/j.jcjp.2023.100117](https://doi.org/10.1016/j.jcjp.2023.100117).

References

- Appel H, Friberg S. The effect of high tibial osteotomy on pain in osteoarthritis of the knee joint. *Acta Orthop*. 1972;43(6):558–565. doi:[10.3109/17453677208991278](https://doi.org/10.3109/17453677208991278).
- Ekhtiari S, Haldane CE, de Sa D, Simunovic N, Musahl V, Ayeni OR. Return to work and sport following high tibial osteotomy: a systematic review. *J Bone Joint Surg - Am*. 2016;98(18):1568–1577. doi:[10.2106/JBJS.16.00036](https://doi.org/10.2106/JBJS.16.00036).
- Lobenhoffer P. Indication for unicompartmental knee replacement versus osteotomy around the knee. *J Knee Surg*. 2017;30(8):769–773. doi:[10.1055/s-0037-1605558](https://doi.org/10.1055/s-0037-1605558).
- van Haeringen MH, Kuijer PPFM, Daams JG, et al. Opening- and closing-wedge high tibial osteotomy are comparable and early full weight bearing is safe with angular stable plate fixation: a meta-analysis. *Knee Surg Sports Traumatol Arthrosc*. 2023. Online ahead of print. doi:[10.1007/s00167-022-07305-8](https://doi.org/10.1007/s00167-022-07305-8).
- Wang Z, Zeng Y, She W, Luo X, Cai L. Is opening-wedge high tibial osteotomy superior to closing-wedge high tibial osteotomy in treatment of unicompartmental osteoarthritis? A meta-analysis of randomized controlled trials. *Int J Surg*. 2018;60:153–163. doi:[10.1016/j.ijsu.2018.10.045](https://doi.org/10.1016/j.ijsu.2018.10.045).
- Lee DC, Byun SJ. High tibial osteotomy. *Knee Surg Relat Res*. 2012;24(2):61–69. doi:[10.5792/ksrr.2012.24.2.61](https://doi.org/10.5792/ksrr.2012.24.2.61).
- Han JH, Kim HJ, Song JG, et al. Is bone grafting necessary in opening wedge high tibial osteotomy? A meta-analysis of radiological outcomes. *Knee Surg Relat Res*. 2015;27(4):207–220. doi:[10.5792/ksrr.2015.27.4.207](https://doi.org/10.5792/ksrr.2015.27.4.207).
- van Genechten W, van den Bempt M, van Tilborg W, et al. Structural allograft impaction enables fast rehabilitation in opening-wedge high tibial osteotomy: a consecutive case series with one year follow-up. *Knee Surg Sports Traumatol Arthrosc*. 2020;28(12):3747–3757. doi:[10.1007/s00167-019-05765-z](https://doi.org/10.1007/s00167-019-05765-z).
- Cao ZW, Mai XJ, Wang J, Feng EH, Huang YM. Uni-compartmental knee arthroplasty versus high tibial osteotomy for knee osteoarthritis: a systematic review and meta-analysis. *J Arthroplasty*. 2018;33(3):952–959. doi:[10.1016/j.arth.2017.10.025](https://doi.org/10.1016/j.arth.2017.10.025).
- Chae DJ, Shetty GM, Lee DB, Choi HW, Han SB, Nha KW. Tibial slope and patellar height after opening wedge high tibia osteotomy using autologous tricortical iliac bone graft. *Knee*. 2008;15(2):128–133. doi:[10.1016/j.knee.2007.11.001](https://doi.org/10.1016/j.knee.2007.11.001).
- Lee JS, Park YJ, Wang L, Chang YS, Shetty GM, Nha KW. Modified iliac crest reconstruction with bone cement for reduction of donor site pain and morbidity after open wedge high tibial osteotomy: a prospective study. *Knee Surg Relat Res*. 2016;28(4):277–282. doi:[10.5792/ksrr.15.046](https://doi.org/10.5792/ksrr.15.046).
- Kuremsky MA, Schaller TM, Hall CC, Roehr BA, Masonis JL. Comparison of autograft vs allograft in opening-wedge high tibial osteotomy. *J Arthroplasty*. 2010;25(6):951–957. doi:[10.1016/j.arth.2009.07.026](https://doi.org/10.1016/j.arth.2009.07.026).
- Lode A, Meissner K, Luo Y, et al. Fabrication of porous scaffolds by three-dimensional plotting of a pasty calcium phosphate bone cement under mild conditions. *J Tissue Eng Regen Med*. 2014;8(9):682–693. doi:[10.1002/term.1563](https://doi.org/10.1002/term.1563).
- Hooper NM, Schouten R, Hooper GJ. The outcome of bone substitute wedges in medial opening high tibial osteotomy. *Open Orthop J*. 2013;7(1):373–377. doi:[10.2174/1874325001307010373](https://doi.org/10.2174/1874325001307010373).
- Castilho M, Moseke C, Ewald A, et al. Direct 3D powder printing of biphasic calcium phosphate scaffolds for substitution of complex bone defects. *Biofabrication*. 2014;6(1). doi:[10.1088/1758-5082/6/1/015006](https://doi.org/10.1088/1758-5082/6/1/015006).
- Yang X, Xie B, Wang L, Qin Y, Henneman ZJ, Nancollas GH. Influence of magnesium ions and amino acids on the nucleation and growth of hydroxyapatite. *CrystEngComm*. 2011;13(4):1153–1158. doi:[10.1039/c0ce00470g](https://doi.org/10.1039/c0ce00470g).
- Yang F, Yang D, Tu J, Zheng Q, Cai L, Wang L. Strontium enhances osteogenic differentiation of mesenchymal stem cells and in vivo bone formation by activating Wnt/catenin signaling. *Stem Cells*. 2011;29(6):981–991. doi:[10.1002/stem.646](https://doi.org/10.1002/stem.646).
- Reitmaier S, Kovtun A, Schuelke J, et al. Strontium(II) and mechanical loading additively augment bone formation in calcium phosphate scaffolds. *J Orthop Res*. 2018;36(1):106–117. doi:[10.1002/jor.23623](https://doi.org/10.1002/jor.23623).
- Lode A, Heiss C, Knapp G, et al. Strontium-modified premixed calcium phosphate cements for the therapy of osteoporotic bone defects. *Acta Biomater*. 2018;65:475–485. doi:[10.1016/j.actbio.2017.10.036](https://doi.org/10.1016/j.actbio.2017.10.036).
- Kim JA, Lim J, Naren R, suk Yun H, Park EK. Effect of the biodegradation rate controlled by pore structures in magnesium phosphate ceramic scaffolds on bone tissue regeneration in vivo. *Acta Biomater*. 2016;44:155–167. doi:[10.1016/j.actbio.2016.08.039](https://doi.org/10.1016/j.actbio.2016.08.039).
- Jia J, Zhou H, Wei J, et al. Development of magnesium calcium phosphate biocement for bone regeneration. *J R Soc Interface*. 2010;7(49):1171–1180. doi:[10.1098/rsif.2009.0559](https://doi.org/10.1098/rsif.2009.0559).
- Ostrowski N, Roy A, Kumta PN. Magnesium phosphate cement systems for hard tissue applications: a review. *ACS Biomater Sci Eng*. 2016;2(7):1067–1083. doi:[10.1021/acsbomaterials.6b00056](https://doi.org/10.1021/acsbomaterials.6b00056).
- Golafshan N, Vorndran E, Zaharievski S, et al. Tough magnesium phosphate-based 3D-printed implants induce bone regeneration in an equine defect model. *Biomaterials*. 2020;261:120302. doi:[10.1016/j.biomaterials.2020.120302](https://doi.org/10.1016/j.biomaterials.2020.120302).
- Lobenhoffer P, Agneskirchner JD. Improvements in surgical technique of valgus high tibial osteotomy. *Knee Surg Sports Traumatol Arthrosc*. 2003;11(3):132–138. doi:[10.1007/s00167-002-0334-7](https://doi.org/10.1007/s00167-002-0334-7).
- Sasaki S, Maeyama A, Kiyama T, et al. Combined use of beta-tricalcium phosphate with different porosities can accelerate bone remodelling in open-wedge high tibial osteotomy. *Asia Pac J Sports Med Arthrosc Rehab Technol*. 2022;29:30–34. doi:[10.1016/j.asmart.2022.05.004](https://doi.org/10.1016/j.asmart.2022.05.004).
- Koh YG, Kwon OR, Kim YS, Choi YJ. Comparative outcomes of open-wedge high tibial osteotomy with platelet-rich plasma alone or in combination with mesenchymal stem cell treatment: A prospective study. *Arthroscop - J Arthroscop Related Surg*. 2014;30(11):1453–1460. doi:[10.1016/j.arthro.2014.05.036](https://doi.org/10.1016/j.arthro.2014.05.036).
- Chiari C, Grgurevic L, Bordukalo-Niksic T, et al. Recombinant human BMP6 applied within autologous blood coagulum accelerates bone healing: randomized controlled trial in high tibial osteotomy patients. *J Bone Mineral Res*. 2020;35(10):1893–1903. doi:[10.1002/jbmr.4107](https://doi.org/10.1002/jbmr.4107).
- Gerhardt LC, Boccacini AR. Bioactive glass and glass-ceramic scaffolds for bone tissue engineering. *Materials*. 2010;3(7):3867–3910. doi:[10.3390/ma3073867](https://doi.org/10.3390/ma3073867).
- Fortier LA, Strauss EJ, Sheppard DO, Beckett L, Kennedy JG. Biological effects of bone marrow concentrate in knee pathologies. *J Knee Surg*. 2019;32(1):2–8. doi:[10.1055/s-0038-1676069](https://doi.org/10.1055/s-0038-1676069).
- Willemsen K, Nizak R, Noordmans HJ, Castelein RM, Weinans H, Kruyt MC. Challenges in the design and regulatory approval of 3D-printed surgical implants: a two-case series. *Lancet Digit Health*. 2019;1(4):e163–e171. doi:[10.1016/S2589-7500\(19\)30067-6](https://doi.org/10.1016/S2589-7500(19)30067-6).
- Willemsen K, Tryfonidou M, Sakkers R, et al. Patient-specific 3D-printed shelf implant for the treatment of hip dysplasia: anatomical and biomechanical outcomes in a canine model. *J Orthop Res*. 2022;40(5):1154–1162. doi:[10.1002/jor.25133](https://doi.org/10.1002/jor.25133).